

Acid Catalysis Mediated by Aqueous Hydronium Ions Formed by Contacting Zeolite Crystals with Liquid Water

Yue Liu, Chen Luo, Shuai Wang, Enrique Iglesia,* and Haichao Liu*



Cite This: *J. Am. Chem. Soc.* 2024, 146, 35185–35198



Read Online

ACCESS |



Metrics & More

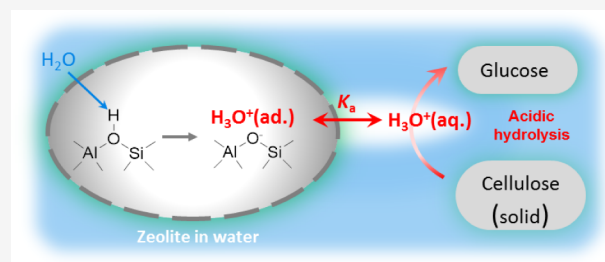


Article Recommendations



Supporting Information

ABSTRACT: Zeolites are crystalline microporous aluminosilicates widely used as solid acids in catalytic routes to clean and sustainable energy carriers and chemicals from biogenic and fossil feedstocks. This study addresses how zeolites act as weak polyprotic acids and dissociate to form extra-crystalline hydronium (H_3O^+) ions in liquid water. The extent of their dissociation depends on the energy required to form the conjugate framework anions, which becomes unfavorable as the extent of dissociation increases intracrystalline charge densities because repulsive interactions ultimately preclude the detachment of all protons as catalytically relevant $\text{H}_3\text{O}^+(\text{aq})$ ions. The extent of dissociation is accurately described using electrostatic repulsion formalisms that account for aqueous H_3O^+ concentrations for all zeolite concentrations, Al densities, and frameworks. Probed by hydrolysis of cellulose, the most abundant biogenic polymer, this study demonstrates that zeolites catalyze this reaction exclusively through the formation of the extra-crystalline H_3O^+ ions at rates strictly proportional to their concentrations in the aqueous phase, irrespective of their provenance from zeolites differing in framework structure or Al content, without the purported involvement of acid sites at extracrystalline surfaces or intervening formation of smaller cellulose oligomers. The results and mechanistic interpretations seamlessly and rigorously bridge the chemistry of solid and liquid acids in aqueous media, while resolving the enduring puzzle of solid acids that catalyze transformations of substrates that cannot enter the voids where acid sites reside.



INTRODUCTION

Zeolites consist of aluminosilicate frameworks with voids of molecular dimensions and a negatively charged framework balanced by grafted cations. When these grafted cations are protons, they act as solid acids that are widely used as catalysts in processes for the synthesis and upgrading of energy carriers and chemicals, such as transformations of hydrocarbons,^{1–6} synthesis gas mixtures,^{7–10} methanol^{11–13} and CO_2 ,^{14,15} as well as in the chemical recycling of plastic wastes.^{16,17} Their acid properties are conferred by these protons, which reside predominantly within their void space and balance the charge created by the isomorphic substitution of Al^{3+} for Si^{4+} into neutral silicate frameworks; their Brønsted acid function is complemented by concerted van der Waals interactions between the host framework and guest organic molecules involved as intermediates and transition states in catalytic reactions. These confinement effects confer the remarkable catalytic diversity that characterizes zeolitic solid acids in practice.¹⁸ Lewis acid centers, as Al atoms detached from the framework (extra framework Al) are also present in these materials and can act as a distinct type of binding site.^{18–20} The type and number of acid sites, together with the ubiquitous effects of confinement, determine the properties of these materials as catalysts. In some cases, as in this study, the role of the zeolite is merely to dissociate into anionic frameworks and aqueous H_3O^+ species, for which confinement

effects are no longer consequential for any reactant molecules that cannot plausibly enter their voids, but which react instead using the acid function provided by the zeolites through their dissociation into aqueous hydronium ions.

Here, the hydrolytic conversion of cellulosic materials,^{21–23} a biogenic source of carbon, is examined using zeolitic acids immersed in liquid water, as well as mineral acids. Cellulose is a water-insoluble oligomer of glucose units linked by β -1,4-glucoside bonds.²⁴ It is efficiently hydrolyzed by acids, such as zeolites, to form glucose.^{25,26} Hydrolysis requires the protonation of glucoside bonds and the subsequent H_2O -mediated cleavage of the C–O–C moieties that link glucose subunits. The observed hydrolysis, once implausibly proposed to be mediated by intracrystalline protons (present within voids smaller than 0.5–1 nm) cannot possibly involve protons within such voids because of the inaccessibility of cellulose (an insoluble polymer containing 300–10,000 glucose subunits),²⁷ but its mechanistic basis remains an enduring puzzle. Yet, this

Received: August 27, 2024

Revised: November 28, 2024

Accepted: December 2, 2024

Published: December 12, 2024



Table 1. Brønsted Acid Site (BAS) Density in Zeolites, Cellulose Conversion and Polyol Selectivities

Zeolite	Si/Al ratio	BAS density (ρ_B) ^a (BAS nm ⁻³)	Cellulose conversion (%) ^b	Selectivity (%)				
				Ethylene glycol	Triols ^c	Tetritols ^d	Pentitols ^e	Hexitols ^f
None			12.5	7.5	6.3	3.2	10.3	64.7
H-MFI(16) ^g	16	0.91	30.6	4.6	4.7	0.7	5.5	56.0
H-MFI(21) ^g	21	0.75	28.0	4.8	5.0	0.8	6.9	61.7
H-MFI(58) ^g	58	0.31	23.4	5.5	5.8	2.2	6.0	63.1
H-MFI(100) ^g	100	0.18	21.0	7.2	6.3	1.7	3.2	54.4
H-BEA	14	0.87	30.8	5.3	4.6	1.0	4.9	55.7
H-MOR	12	1.19	27.7	6.3	5.3	1.1	7.7	61.4
H-FAU	13	0.42	28.8	6.2	5.4	1.6	7.5	55.0

^aBAS density measured from the amount of NH₃ evolved from NH₄-zeolites. ^bBatch stirred reactor; 478 K, 0.5 h, 6 MPa H₂, 40 g water, 0.2 g zeolite, 1.0 g cellulose, 0.02 g 3 wt % Ru/C. ^cPropylene glycol and glycerol. ^dErythritol and threitol. ^eRibitol, arabitol and xylitol. ^fSorbitol, mannitol and iditol. ^gNumbers in parentheses refer to the Si/Al ratio measured by X-ray fluorescence spectra.

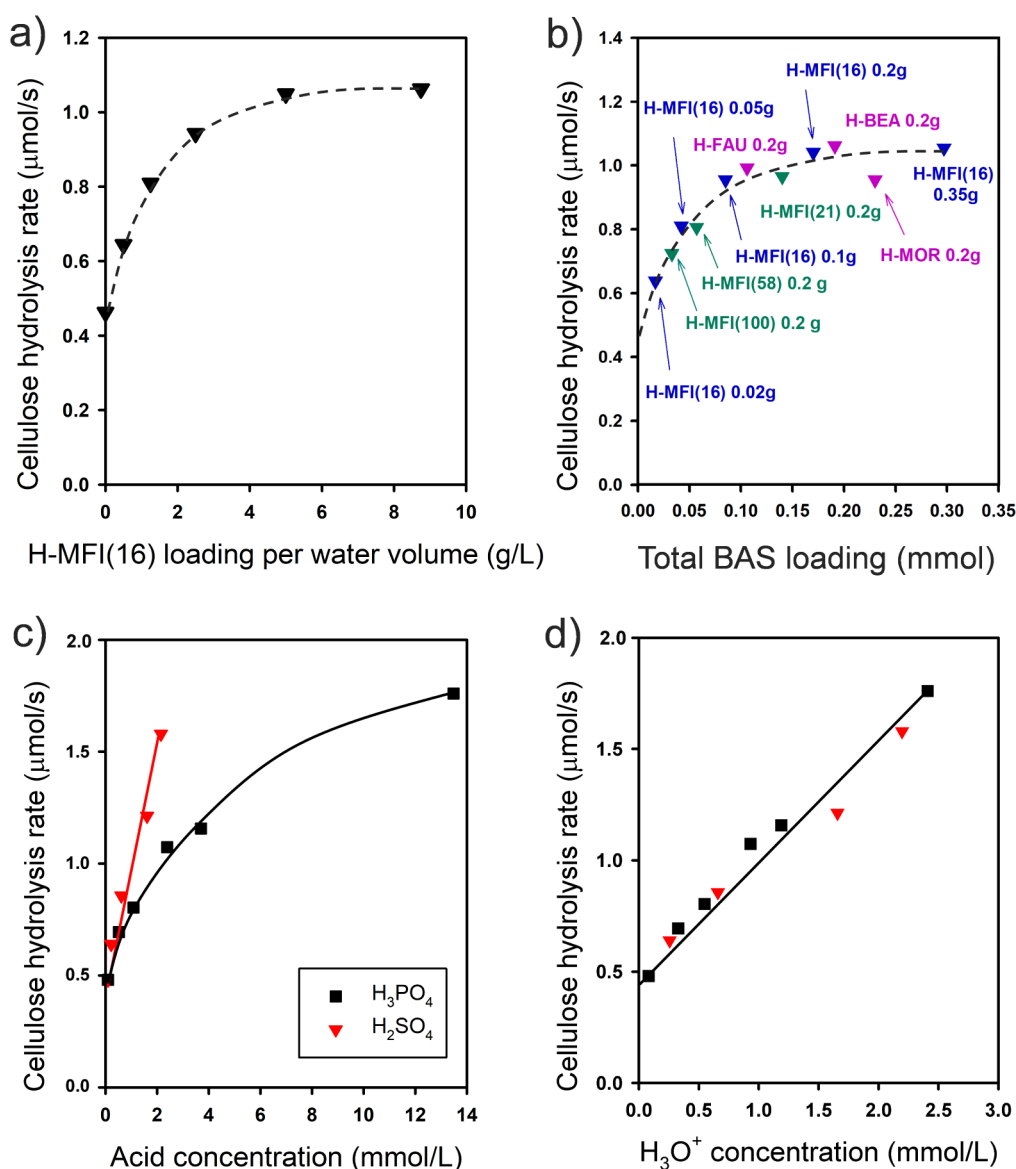
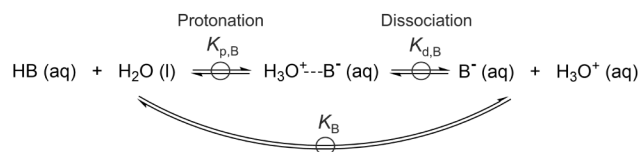
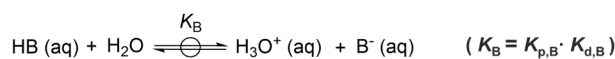


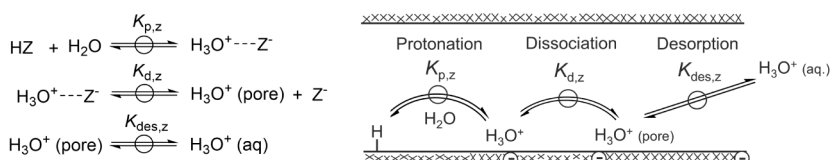
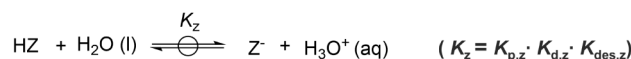
Figure 1. (a) Cellulose hydrolysis rate with different amounts of H-MFI(16) used per volume of water. (b) Cellulose hydrolysis rate as a function of total BAS numbers for different zeolites. (c) Cellulose hydrolysis rate as a function of H₃PO₄ and H₂SO₄ concentrations. (d) Cellulose hydrolysis rate as a function of hydronium H₃O⁺ concentration in aqueous H₃PO₄ and H₂SO₄ solutions (478 K, 30 min, 6 MPa H₂, 40 g water, 1.0 g cellulose, 0.02 g 3 wt.% Ru/C). The H₃O⁺ concentration for H₃PO₄ and H₂SO₄ in (d) is calculated based on their dissociation constants and properties of water at each reaction temperature.^{37,41,42}

Scheme 1. Schematic Depiction of Dissociation Processes for Mineral Acids and Zeolitic Acids in Aqueous Media

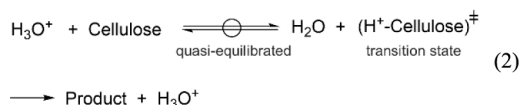
a) Mineral acids



b) Zeolitic solid acids



Cellulose conversion rates are limited by its initial acid-catalyzed hydrolysis step. In aqueous media, such steps first require a reaction between cellulose and H_3O^+ ions via a protonated cellulose moiety at the transition state (\ddagger , eq 2):



Cellulose hydrolysis rates can be expressed using the tenets of transition state theory as (details of the derivation in Section S1):

$$r = \frac{k_B T}{h} \exp\left(-\frac{\Delta G^\ddagger}{RT}\right) c_{\text{H}^+} c_{\text{cellulose}} \quad (3)$$

where C_{H^+} and $c_{\text{cellulose}}$ represent the concentration of H_3O^+ ions and cellulose in aqueous media, respectively; ΔG^\ddagger is the activation Gibbs free energy of formation of the transition state from cellulose and H_3O^+ ions.

Table 1 shows cellulose conversions and selectivities to polyols for reactions in liquid water (40 g) at 478 K and 6 MPa H_2 on Ru/C catalysts with and without the presence of various zeolites in their H-form (H-MOR, H-BEA, H-FAU and H-MFI; 0.2 g zeolite). The Si/Al ratio and the Brønsted acid site (BAS) density are also listed in Table 1 for each zeolite sample used in this study. In the absence of zeolites, the cellulose conversion in water was 12.5% after 0.5 h; these rates reflect the prevalent concentration of H_3O^+ ions in pure liquid water, given by its temperature-dependent equilibrium dissociation constant.³⁷ Hexitols, predominantly sorbitol and mannitol, were the predominant products (64.7%; Table 1), consistent with previous studies.³⁸ Ethylene glycol (7.5%), triols (6.3%), tetritols (3.2%), and pentitols (10.3%) were also detected in the reaction on Ru/C catalysts dispersed in water but without the presence of zeolites.

The addition of H-zeolites increased cellulose conversion levels (to 30.6% after 0.5 h in the case of H-MFI (Si/Al 16)), and the hexitol selectivities slightly decreased (e.g., from 64.7% to 56.0% on H-MFI(16) at about 30% conversion) because of subsequent acid-catalyzed dehydration of sorbitol and mannitol.^{39,40} The higher cellulose conversions and similar

distributions of hydrogenation products (polyols) on all zeolites, compared with those in pure water, confirm the catalytic role of zeolites in cellulose hydrolysis and in mediating the kinetically relevant step involved in the formation of all hydrogenated products in these cascade reactions.

Figure 1a depicts cellulose hydrolysis rates that increase linearly with the amount of H-MFI(16) charged (per water volume) at low catalyst concentrations, but then reaches nearly constant values ($1.0 \mu\text{mol s}^{-1}$, all rates are defined as the moles of cleaved glycosidic bonds per s) above 5.0 g L^{-1} . Such trends are unaffected (Figure 1b) by whether the proton density (per H_2O volume) was varied through changes in the framework identity (H-MFI, H-BEA, H-MOR, H-FAU; Figure 1b) or the BAS concentration for any given zeolite framework ($0.18\text{--}0.91 \text{ BAS nm}^{-3}$ for H-MFI). It is evident that cellulose hydrolysis rates are not strictly proportional to the mass of the purported catalyst charged, even though this is the accepted requirement for a reaction to be mediated by the catalyst and for the absence of diffusional artifacts.

Cellulose hydrolysis rates were also measured on aqueous mineral acids (H_3PO_4 , H_2SO_4) at 478 K. An increase in H_3PO_4 concentrations from 0 to about 0.5 mM led to a linear increase in cellulose hydrolysis rates, but to a sublinear increase at higher H_3PO_4 concentrations (2–14 mM; Figure 1c). In contrast, rates increased linearly with H_2SO_4 concentration throughout the entire concentration range (0–2 mM; Figure 1c). These different trends reflect the incomplete dissociation of the weaker H_3PO_4 acids; both mineral acids (H_3PO_4 and H_2SO_4), however, gave similar hydrolysis rates when rates were normalized by their respective $\text{H}_3\text{O}^+(\text{aq})$ concentrations (determined from their pH values). For both acids, rates were the same at any given concentration of hydronium ions and increased linearly with $\text{H}_3\text{O}^+(\text{aq})$ concentration ($<2.3 \text{ mM}$) at all H_3PO_4 and H_2SO_4 concentrations. At these dilute H_3O^+ concentrations ($<2.5 \text{ mM}$), the H_3O^+ activity coefficients are near unity (γ_{H^+} : 0.92–0.98 for 0.1–2.5 mM H_3O^+ , 478 K), as evident from Debye–Hückel formalisms for dilute strong electrolytes (details in Section S2). These data for mineral acids give a value of the intrinsic reactivity of aqueous H_3O^+ with a rate constant of $0.086 \text{ L mol}^{-1} \text{ s}^{-1}$ (based on eq 3;

478 K); these constant turnover rates are indicative of the direct involvement and equal reactivity of aqueous hydronium ions (irrespective of provenance or concentration) in the kinetically-relevant steps that mediate cellulose hydrolysis.

The absence of a linear dependence of cellulose hydrolysis rates on the number of protons in the amount of zeolite present (Figure 1b) resembles those expected (and observed, Figure 1c) for weak acids, such as H_3PO_4 . These trends indicate that zeolite crystals merely behave as polyprotic acids of modest strength, which dissociate incompletely in aqueous media at the conditions of reaction. As a result, $\text{H}_3\text{O}^+(\text{aq})$ concentrations depend not only on their acid dissociation constants (and thus on acid strength), but also on the relative proportion of water and solids prevalent in the reaction suspension, as is the case for weak mineral acids, where the combined effects of dissociation constants and acid amounts determine H_3O^+ concentrations. Only the H_3O^+ ions in the extracrystalline water phase are responsible for hydrolysis of cellulosic moieties that cannot access intracrystalline bound protons or confined H_3O^+ ions within zeolites. This conclusion leads, in turn, to the prediction that hydrolysis rates would depend linearly on the concentration of aqueous H_3O^+ ions, irrespective of their provenance from the dissociation of liquid water, mineral acids, or zeolites crystallites.

Next, these extracrystalline concentrations of aqueous H_3O^+ ions are described using concepts first developed for the incomplete ionization of weak mineral acids. These concepts are then used to show that cellulose hydrolysis rates are independent of the type, amount, or Al content in zeolites, but similar to those for mineral acids and solely dependent on the prevalent aqueous H_3O^+ concentrations in the extracrystalline aqueous media.

Theoretical Assessments of the Dissociation of Intracrystalline O–H Groups and of Their Equilibration with Extracrystalline H_3O^+ Ions in Aqueous Media. *Dissociation of Acid Zeolites in Aqueous Media.* The dissociation of weak monoprotic acids occurs via the stabilization of protons by H_2O molecules to form H_3O^+ complexes that interact with the conjugate bases (B^-) and with the H-bonded H_2O network, but which ultimately dissociate the proton-base pair to gain the entropy of mixing that compensates for the enthalpic cost of dissociation (Scheme 1a). The equilibrium $K_{\text{p,B}}$ for the local protonation to form the H_3O^+ species bound at the conjugate base and $K_{\text{d,B}}$ for its dissociation (the desorption of bound H_3O^+ ions into the aqueous phase). The overall equilibrium constant K_{B} for the dissociation of mineral acids (Scheme 1a) is the product of $K_{\text{p,B}}$ and $K_{\text{d,B}}$ ($K_{\text{B}} = K_{\text{p,B}} \cdot K_{\text{d,B}}$).

A similar formalism and sequence of equilibrated steps (Scheme 1b) describe the thermodynamics of detachment of protons from its solid conjugate base in the case of solid acids, specifically in this case, from the anionic framework of a zeolite crystal. Dissociation involves: (i) protonation of H_2O to form H_3O^+ ions bound at the conjugate zeolite framework ($K_{\text{p,z}}$); (ii) detachment of H_3O^+ from the framework (Z^-) to form H_3O^+ species that remain solvated within intracrystalline voids ($\text{H}_3\text{O}^+(\text{pore})$; $K_{\text{d,z}}$); and (iii) desorption of $\text{H}_3\text{O}^+(\text{pore})$ ions into the extracrystalline bulk aqueous phase to form $\text{H}_3\text{O}^+(\text{aq})$ ions ($K_{\text{des,z}}$). The overall equilibrium dissociation constant K_{z} therefore reflects the product of the three constants ($K_{\text{z}} = K_{\text{p,z}} \cdot K_{\text{d,z}} \cdot K_{\text{des,z}}$).

The overall dissociation constants (K_{B} for mineral acids in Scheme 1a; K_{z} for H-zeolites in Scheme 1b) then give the equilibrium relations:

$$K_{\text{B}} = \frac{a_{\text{H}^+} a_{\text{B}^-}}{a_{\text{HB}}} = \frac{\gamma_{\text{H}^+} \gamma_{\text{B}^-}}{\gamma_{\text{HB}}} \cdot \frac{c_{\text{H}^+} \alpha}{1 - \alpha} \cdot \frac{1}{c^\circ} \quad (4a)$$

$$K_{\text{z}} = \frac{a_{\text{H}^+} a_{\text{Z}^-}}{a_{\text{HZ}}} = \frac{\gamma_{\text{H}^+} \gamma_{\text{Z}^-}}{\gamma_{\text{HZ}}} \cdot \frac{c_{\text{H}^+} \alpha}{1 - \alpha} \cdot \frac{1}{c^\circ} \quad (4b)$$

In these equations, a_{H^+} , c_{H^+} and γ_{H^+} represent the activity, concentration, and activity coefficients for H_3O^+ ions, respectively, in the aqueous media; a_{HB} and a_{B^-} represent the activities of the mineral acid HB and the conjugate base B^- solvated by the aqueous media, and the γ_{HB} and γ_{Z^-} terms are their respective activity coefficients, c° is the standard state concentration (1 mol L^{-1}). The a_{HZ} and a_{Z^-} terms are the thermodynamic activities of the HZ acid moiety in the aluminosilicates and of their conjugate anions (anionic framework with Al–O–Si sites), while γ_{HZ} and γ_{Z^-} are their respective activity coefficients. In addition, the degree of dissociation (α) is defined here as the ratio of the number of B^- anions present to the number of HB initially present in the undissociated mineral acid; it represents the ratio of the number of dissociated zeolitic Brønsted acid sites (Z^-) to the initial number of protons in H-zeolites. Accordingly, the term $(1 - \alpha)$ represents the fraction of the protons that remain associated with the respective framework conjugate bases or confined as H_3O^+ within the zeolite micropores (only the former for mineral acids).

For H-zeolites, the geometric structure of the dissociated acid site (Z^-) is essentially unchanged by deprotonation and thus resembles that for its undissociated form (HZ); it differs only in its negative charge. Therefore, its activity coefficient γ_{Z^-} can be accurately dissected into the product of γ_{HZ} and of an activity coefficient ($\gamma_{-(z)}$) that accounts for the nonidealities imposed by interactions with the surrounding environment specifically mediated by the presence of such negative charges ($\gamma_{\text{Z}^-} = \gamma_{-(z)} \cdot \gamma_{\text{HZ}}$). Similarly, the activity coefficient (γ_{B^-}) of mineral acids is also expressed as the product of γ_{HB} and $\gamma_{-(\text{B})}$ ($\gamma_{\text{B}^-} = \gamma_{-(\text{B})} \cdot \gamma_{\text{HB}}$). In addition, Debye–Hückel formalisms for dilute electrolytes indicate that activity coefficients for aqueous H_3O^+ ions are near unity at their low prevalent concentrations for all solid acids and dilute mineral acids examined in this study ($<2.3 \text{ mM H}_3\text{O}^+$; γ_{H^+} from zeolite: 0.98–0.99 at 298 K and 0.96–0.99 at 478 K; γ_{H^+} from mineral acid: 0.92–0.98 at 478 K; calculation details are shown in Section S2 and S3). eq 4a then becomes

$$\alpha = \frac{K_{\text{B}}}{\frac{c_{\text{H}^+}}{c^\circ} + K_{\text{B}}} \quad (5a)$$

$$\alpha = \frac{K_{\text{z}}}{\frac{c_{\text{H}^+}}{c^\circ} \gamma_{-(z)} + K_{\text{z}}} \quad (5b)$$

Equation 5a shows that for strong mineral acids, their large K_{B} values allow complete dissociation for a broad range of c_{H^+} (e.g., H_2SO_4) but not for weak acids, which show a decrease in α as c_{H^+} (e.g., H_3PO_4). These trends reflect the decreasing contributions from the entropy of mixing to the dissociation free energies as c_{H^+} increases ($-RT \ln(C_{\text{H}^+})$) and their ultimate

inability to compensate for the larger dissociation enthalpy of the weaker acids.

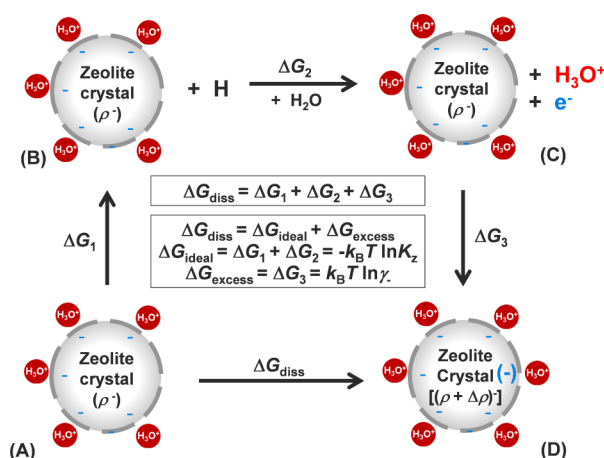
These entropy contributions are also prevalent in the dissociation of zeolitic acids in aqueous media and influence K_z values, but α values are additionally (and strongly) influenced by the accumulation of charge reflected in $\gamma_{-(z)}$ (eq 5b), a term that reflects the electrostatic repulsion caused by the accumulation of negative charges within zeolite crystals. Such effects, albeit at smaller distances, are also evident in the much smaller K_B values as protons are additionally removed from polyprotic molecular and mineral acids. For instance, these K_B values decrease from 7.9×10^{-3} to 6.3×10^{-8} to 4.0×10^{-13} as protons are removed from H_3PO_4 (298 K).⁴¹ This is also the case for polyprotic heteropolyacids ($\text{H}_3\text{PW}_{12}\text{O}_{40}$ in acetone, from 2.5×10^{-2} to 1.0×10^{-3} to 1.0×10^{-4} , 298 K),⁴³ for which such effects are weaker because the negative charge is delocalized over a much larger oxide domain than for H_3PO_4 acids.

Thermodynamic Treatments of Zeolite Dissociation in Aqueous Media. A monoprotic mineral acid dissociates in aqueous media into an anion and a cation ($\text{H}_3\text{O}^+(\text{aq})$) both present in dilute form for the systems of interest in this study. Analogously, protons within zeolite frameworks can detach from the conjugate anion to form dilute $\text{H}_3\text{O}^+(\text{aq})$ ions and negatively charged frameworks. Each zeolite crystal, however, contains many protons. For instance, H-MFI crystals with a Si/Al ratio of 10 and $1 \mu\text{m}^3$ volume contain 1.6×10^9 BAS and a volumetric density of 1.6 BAS nm^{-3} , corresponding to a mean distance of 0.85 nm among BAS in the undissociated zeolite. This leads to a significant anion density as dissociation occurs. In contrast with monoprotic mineral acids dispersed in solution, these charges accumulate inside zeolite crystals at densities that cause significant electrostatic repulsion, causing $\gamma_{-(z)}$ values to increase sharply above unity as the extent of dissociation increases. The concomitant repulsion destabilizes the conjugate anion until equilibrium is reached as these electrostatic forces (together with the intrinsic dissociation enthalpy for a zeolitic proton) can no longer be compensated by the entropy of mixing as $\text{H}_3\text{O}^+(\text{aq})$ ions enter the extracrystalline fluid phase.

The Gibbs free energy changes associated with these dissociation events are dissected using a Born–Haber thermodynamic cycle for the detachment of protons from zeolite frameworks, as described in Scheme 2 and discussed in detail below.

This Born–Haber formalism (Scheme 2) divides the detachment process into hypothetical individual steps that complete a detachment event by considering a zeolite crystal immersed in liquid water and having a total negative charge N (H-Z^{N-}) distributed uniformly throughout its volume with a charge density ρ . The balancing H_3O^+ ions removed to create this negative charge reside within the extracrystalline aqueous phase and are located at essentially noninteracting distances from the crystal (when uniformly distributed in the liquid through vigorous agitation). The detachment of a proton from a zeolite crystal at a given dissociation extent of α ($\text{H-Z}^{N-} \rightarrow \text{H}^+ + \text{Z}^{(N+1)-}$) is treated in the thermochemical cycle as consisting of three hypothetical steps (Scheme 2, A \rightarrow D); these steps are chosen arbitrarily but they must complete the dissociation event. These steps are chosen for convenience and exploit the state function nature of thermodynamic properties; they consist of:

Scheme 2. Thermodynamic Cycle for Zeolite Dissociation in an Aqueous Phase^a



^aThe hydronium ions (H_3O^+) are at non-interacting distance from the zeolite surface.

- the detachment of a neutral H-atom from a random location within the crystal and its placement within the aqueous phase with a free energy change ΔG_1 (Scheme 2, A \rightarrow B);
- the removal of an electron from this H-atom to a noninteracting location and the solvation of the H^+ ion to form $\text{H}_3\text{O}^+(\text{aq})$ with a free energy change of ΔG_2 (Scheme 2, B \rightarrow C); and
- the placement of the electron removed from the H-atom within a crystal with a pre-existing negative charge (Scheme 2, C \rightarrow D; ΔG_3 for the total energy change).

The total dissociation free energy change is then given by the sum of these individual free energies, because they complete a dissociation event:

$$\Delta G_{\text{diss}} = \Delta G_1 + \Delta G_2 + \Delta G_3 \quad (6)$$

The ΔG_1 and ΔG_2 terms do not depend on the charge density within a zeolite crystal and are thus insensitive to the extent of dissociation. In contrast, ΔG_3 equals the sum of the work (W) required to move an electron from a noninteracting distance into a crystal with a given preexisting negative charge density (set by the extent of dissociation) while maintaining all aqueous H_3O^+ ions at noninteracting distance. Consequently, ΔG_3 increases as the preexisting charge present in the crystal increases. The sum of ΔG_1 and ΔG_2 reflects only the ideal state contributions to ΔG_{diss} , whereas ΔG_3 represents electrostatic energies from anion–anion interactions that introduce non-idealities, captured, by convention, as the excess free energy (ΔG_{excess}):

$$W = \Delta G_3 = \Delta G_{\text{excess}} = k_B T \ln \gamma_{-(z)} \quad (7)$$

The work term (W) is that required to accumulate negative charges within zeolite crystals. Thus, it is the sum of electrostatic energies from Coulomb interactions among all negative charges. For a negative charge in a wet zeolite crystal, its electrostatic energy (u) by interaction with all the other negative charges is given by the integral:

$$u = \int_{r_0}^{+\infty} u_r \cdot \rho_- 4\pi r^2 dr \quad (8)$$

The term u_r is its Coulomb interaction energy with another negative charge at a distance of r ; ρ_- is the volumetric density of negative charges in the zeolite, and the term $\rho_- 4\pi r^2 dr$ accounts for the number of negative charges at the distance r . The integration should start from the boundary of the negative charge center, which is denoted as r_0 in eq 8. We surmise that in zeolites, r_0 is given by the length of Al–O bond (~ 0.16 nm in $-\text{O}-\text{Al}-\text{O}^-$), because the framework negative charge reflects the replacement of Si^{4+} by Al^{3+} in the framework with the charge delocalized among the four Al–O bonds.

For a volume in space with N negative charges, the total electrostatic energy (U) is proportional to the electrostatic energy of each negative charge (u), given by eq 9a, and the work (W) required to increase the negative charge by one elementary charge unit (eq 9b):

$$U = \frac{1}{2}Nu \quad (9a)$$

$$W = \frac{dU}{dN} \quad (9b)$$

This leads to a W term that is proportional to the dissociation extent α (eq 10, details of the derivation in Section S4):

$$W = \frac{\rho_B q_e^2}{\epsilon_0 \epsilon_z} r_D (r_0 + r_D) \exp\left(-\frac{r_0}{r_D}\right) \cdot \alpha \quad (10)$$

In this equation, ϵ_0 is the vacuum permittivity and ϵ_z is the relative permittivity of the zeolite crystal (ϵ_z) immersed in water; they account for how the electric field among charges decreases with the distance from the charge center in a given medium relative to vacuum; q_e is the elemental charge and ρ_B is the volumetric BAS density. The term r_D represents the Debye length, which accounts for the screening of the negative charges by hydronium ions, present as protonated water clusters and negatively charged framework sites within the zeolite crystal.

Equations 7 and 10 allow $\gamma_{-(z)}$ to be expressed as

$$\gamma_{-(z)} = \exp(\beta \cdot \alpha) \left[\beta = \frac{\rho_B q_e^2}{\epsilon_0 \epsilon_z k_B T} r_D (r_0 + r_D) \exp\left(-\frac{r_0}{r_D}\right) \right] \quad (11)$$

The $\gamma_{-(z)}$ term in eq 5b can be replaced by its form in eq 11 to give:

$$\alpha = \frac{K_z}{\frac{c_{\text{H}^+}}{c^\circ} \exp(\beta \cdot \alpha) + K_z} \quad (12)$$

For $\alpha \ll 1$ (and $\alpha\beta \ll 1$), eq 12 can be simplified into an explicit equation for α as a function of C_{H^+} (eq 13); this equation resembles that for weak mineral acids (eq 5a), but with an additional $(1 + \beta)$ factor:

$$\alpha = \frac{K_z}{\frac{c_{\text{H}^+}}{c^\circ} + (1 + \beta) \cdot K_z} \quad (13)$$

Maximum α values are attained when the aqueous H_3O^+ ion concentrations are much smaller than $(1 + \beta) \cdot K_z$:

$$\alpha_{\text{max}} = \frac{K_z}{(1 + \beta) \cdot K_z} = (1 + \beta)^{-1} \quad (14)$$

The $(1 + \beta)$ value determines the maximum attainable extent of dissociation (α_{max}), thus allowing eq 13 to be rewritten as

$$\alpha = \frac{K_z}{\frac{c_{\text{H}^+}}{c^\circ} + \alpha_{\text{max}}^{-1} \cdot K_z} \quad (15)$$

The values of K_z and α_{max} can be determined by regressing measured values of the extent of dissociation (α) at different concentrations of aqueous H_3O^+ ions (c_{H^+}) to the functional form of eq 12. This is carried out in practice by measuring the pH values at different loadings of zeolite in water (i.e., zeolite mass per water volume), as in the case of mineral acids, in order to obtain α values as a function of c_{H^+} .

The value of K_z is, by its definition, an intrinsic property of a BAS within a zeolite and independent of the charge accumulation within a zeolite crystal. It is, in fact, a measure of the strength of an acid site for each aluminosilicate framework, in a similar manner as K_a values in mineral acids. The effects of charge repulsion are taken into account in the value of α_{max} , which depend on BAS densities (and Si/Al ratios), but not on the framework crystalline structure of the aluminosilicate, as we will show in the next section from the pH measurement of zeolite suspensions in water and the determination of the corresponding K_z and α_{max} on H-MFI, H-BEA, H-FAU and H-BEA.

The Gibbs free energy changes associated with these dissociation events are dissected using a Born–Haber thermodynamic cycle for the detachment of protons from zeolite frameworks, as described in Scheme 2 and discussed in detail below.

Measurements of Extent of Dissociation of Zeolites in Aqueous Media. The pH of well-mixed zeolite suspensions was measured at different zeolite concentrations (zeolite mass per water volume) to determine the extent of dissociation for each zeolite sample and how it depends on the H_3O^+ concentrations in the contacting fluid phase. The introduction of a given amount of zeolite into a known water volume decreased the pH, because of the detachment of protons from zeolite crystals and their incorporation into the extracrystalline aqueous phase, causing the H_3O^+ thermodynamic activity to increase (Figure 2).

Figure 2a shows an illustrative example, in which different amounts of H-MFI(16) were added to H_2O at 298 K and the measured H_3O^+ concentration increased from $5.0 (\times 10^{\pm 0.5}) \times 10^{-4}$ to 0.8 mmol L^{-1} (i.e., pH from 6.3 ± 0.5 to pH 3.2) and then almost unchanged as the H-MFI content increased above 9.0 g L^{-1} . The extent of dissociation (α) for H-MFI(16) for each zeolite amount added (and resulting aqueous H_3O^+ concentration) can be determined from the measured pH through a proton balance:

$$\alpha = \frac{(c_{\text{H}^+} - c_{\text{OH}^-}) \cdot V}{m c_B} \quad (16)$$

where V is the volume of water, m is the zeolite mass, and c_B is the Brønsted acid density per unit mass of zeolite (mol g^{-1}). Figure 2b show that higher aqueous H_3O^+ ion concentrations lead to lower dissociation extents (α), consistent with the functional form of eq 15.

The data in Figure 2b for H-MFI(16) give α_{max} and K_z values of 0.39 ± 0.02 and $(156 \pm 10) \times 10^{-6}$, respectively, when regressed to the functional form of eq 15. This value of α_{max} indicates that only 0.39 of the protons present in this H-

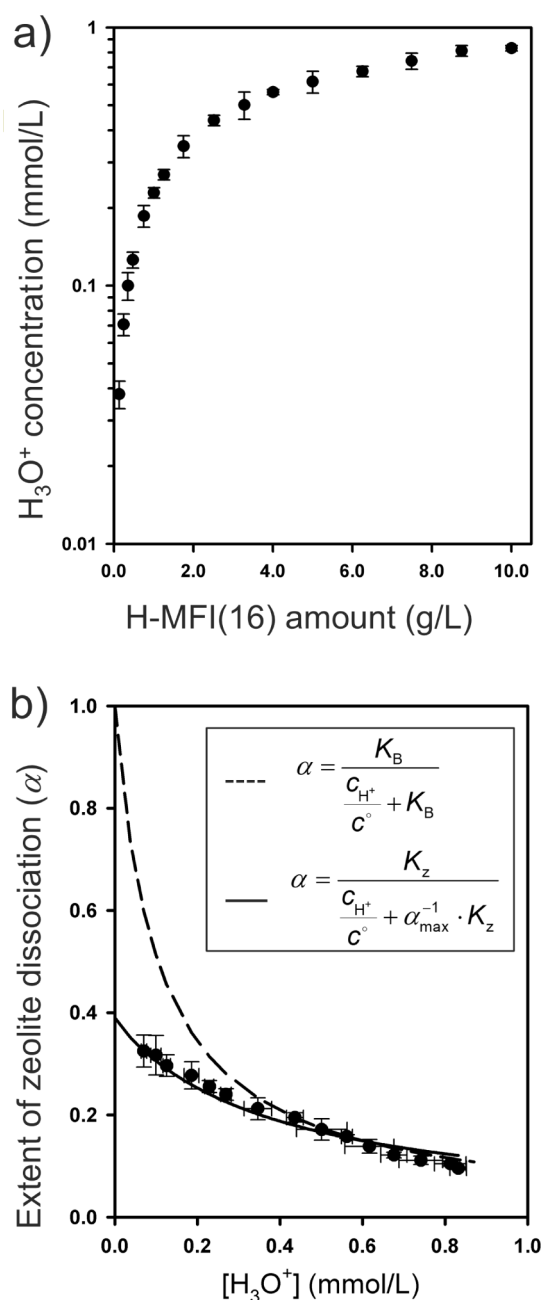


Figure 2. (a) $\text{H}_3\text{O}^+(\text{aq})$ concentrations as a function of H-MFI(16) concentration in water. (b) Extent of zeolitic acid dissociation (α) as a function of H_3O^+ concentration for H-MFI(16). (298 K, 40 g water, 400 rpm agitation speed. H_3O^+ concentrations are changed by varying mass of zeolites loaded in water.).

MFI(16) sample can be detached from framework, even when the $\text{H}_3\text{O}^+(\text{aq})$ concentration in the aqueous phase is very low (<0.1 mmol/L). This contrasts the behavior of mineral acids, even weak ones, which dissociate fully in the asymptotic limit of very dilute $\text{H}_3\text{O}^+(\text{aq})$ ions, because the large (differential) entropy gain upon detachment compensates the dissociation enthalpy so as to provide a favorable free energy. The data in Figure 2b were also regressed using the dissociation equilibrium equation for mineral acids (eq 5a); the resulting fit (dashed curve in Figure 2b) deviates significantly from measured α values.

Accurate descriptions of these effects of H_3O^+ concentration on the extent of dissociation (α) for zeolitic acids require an assessment of the Gibbs free energies contributions from the electrostatic work to accumulate charges within a zeolite crystal (W) and from the entropy gain upon mixing the extracrystalline H_3O^+ into the aqueous phase ($-T\Delta S_m$) for H-MFI(16) at 298 K (eq 17).

$$W = k_B T \ln \gamma_{-(z)} = k_B T \ln \left[\frac{K_z (1 - \alpha) c^\circ}{c_{\text{H}^+} \alpha} \right] \quad (17a)$$

$$\Delta S_m = -R \ln \left(\frac{c_{\text{H}^+}}{c^\circ} \right) \quad (17b)$$

The two contributions are shown separately in Figure 3. The higher H_3O^+ concentrations lead to lower extents of

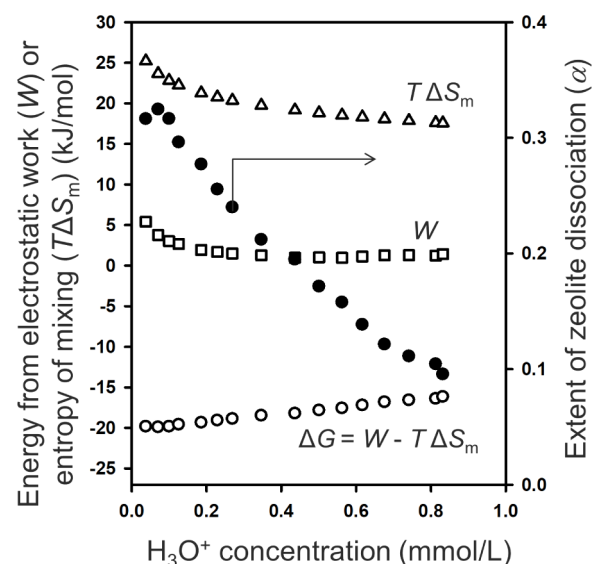


Figure 3. Gibbs free energies ($\Delta G = W - T\Delta S_m$, circle), and contribution from the electrostatic work required to accumulate charges within zeolite crystal (W , square) and from the entropy of mixing H_3O^+ ($T\Delta S_m$, triangle) in bulk water as a function of H_3O^+ concentration for the specific case H-MFI(16). The value of W and ΔS_m are calculate from eqs 17a and 17b.

dissociation (α) and to smaller intracrystalline charge densities and, in turn, to smaller values of the electrostatic work required to remove additional charges from the crystal. At these higher H_3O^+ concentrations, however, the entropy gains upon placing an additional H_3O^+ within the bulk phase are smaller than those at low H_3O^+ concentrations. As a result, entropy gains cannot compensate for the larger amount of work required to detach additional protons from zeolite crystals and these two effects balance to lead to a small dissociation of zeolitic acids. The total Gibbs free energy ($\Delta G = W - T\Delta S_m$), comprising the work and mixing entropy components, changes more weakly with H_3O^+ concentration than the mixing entropy ($T\Delta S_m$), because of the compensation between the two terms of $T\Delta S_m$ and W . In contrast with mineral acids, for which the W term does not depend on the extent of dissociation, this W term increases as charge accumulates within zeolite crystals at higher extents of dissociation. The strong inhibition of dissociation as charge accumulates precludes the detachment of all protons from zeolite frameworks (and solid acids in general). Such trends of α and Gibbs free energy with H_3O^+

concentration for H-MFI (16) are identical for the other zeolites examined, H-MFI(with Si/Al ratios of 21, 58 and 100), H-BEA, H-FAU and H-MOR, as shown below (Figure 4 and Section S6).

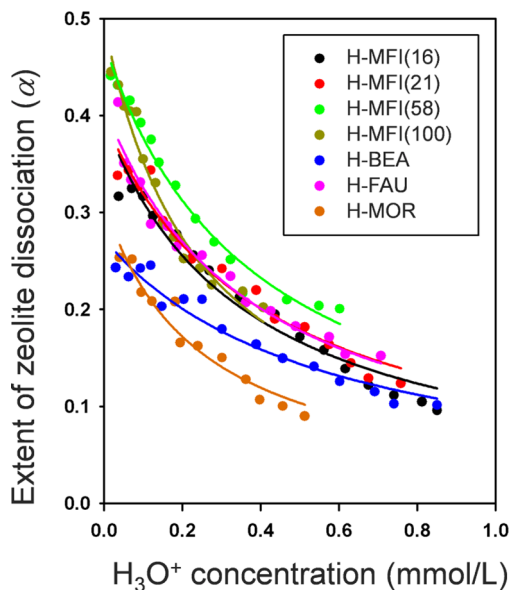


Figure 4. Extent of zeolitic acid dissociation at different H_3O^+ concentrations for H-MFI(with Si/Al of 16, 21, 58 and 100), H-BEA, H-FAU and H-MOR (298 K, 40 g water, 400 rpm agitation speed. H_3O^+ concentrations were varied through changes in the mass of zeolite added to the suspension.) Solid curves represent the regression of the data for each zeolite to the functional form of eq 15 (with the parameters reported in Table 2).

The effects of $\text{H}_3\text{O}^+(\text{aq})$ concentration on α values, shown for H-MFI (16) in Figure 2a, are similar for all framework structures (MFI, BEA, FAU, and MOR) and different Si/Al ratios (16–100 for MFI) examined (Figure 4). The regressed values of α_{max} and K_z for each sample are shown in Table 2.

Table 2. Measured Values of Dissociation Constant K_z and Maximum Dissociation α_{max} for Different Zeolites

zeolite	T (K)	$K_z (\times 10^{-6})$	pK_z^a	α_{max}
H-MFI(16)	298	156 ± 10	3.81 ± 0.03	0.39 ± 0.02
H-MFI(21)	298	163 ± 8	3.79 ± 0.02	0.39 ± 0.02
H-MFI(58)	298	178 ± 9	3.75 ± 0.02	0.48 ± 0.02
H-MFI(100)	298	122 ± 8	3.91 ± 0.03	0.49 ± 0.02
H-MOR	298	78 ± 5	4.11 ± 0.03	0.29 ± 0.01
H-BEA	298	152 ± 10	3.82 ± 0.03	0.28 ± 0.01
H-FAU	298	157 ± 9	3.80 ± 0.03	0.40 ± 0.02
H-MFI(16)	274	140 ± 8	3.85 ± 0.02	0.27 ± 0.02
H-MFI(16)	283	148 ± 9	3.83 ± 0.03	0.34 ± 0.02
H-MFI(16)	313	181 ± 21	3.74 ± 0.05	0.46 ± 0.03

$$^a pK_z = -\log_{10} K_z.$$

The K_z values are similar ($(122\text{--}178) \times 10^{-6}$), as is the case also for their pK_z (i.e., $-\log_{10} K_z$) values (3.74–3.91). Only H-MOR shows a pK_z value that lies outside the uncertainty range of the values measured for other zeolites ($pK_z = 4.11$ for H-MOR); MOR is the only framework with bound H^+ species in two very distinct void environments (12 MR straight channel; 8MR side pockets), of which the smaller 8MR pockets may tend to more strongly retain the hydronium ions via their

stronger constraints, compared to the larger pores of MFI, BEA and FAU. These measured K_z values are much smaller than the K_a values of H_2SO_4 ($K_{a1} = 6.3 \times 10^2$) and H_3PO_4 ($K_{a1} = 7.9 \times 10^{-3}$), making zeolites behave as a weak acid in water.

These data (Figure 4) and their accurate description using eq 15 show that crystalline aluminosilicates in their proton form have acid strengths that are similar for all framework structures (MFI, BEA, FAU and MOR) and Al (and H^+) densities ($0.18\text{--}1.19 \text{ BAS nm}^{-3}$) examined. These data also show that confinement effects do not influence the detachment tendencies of these different aluminosilicates, which merely reflect the equilibration among bound protons and confined and unconfined H_3O^+ ions. Such observations are consistent with the conclusions of theoretical treatments of the acid strength of zeolites in gaseous environments^{44–46} and with measured rates and kinetic trends for methanol dehydration,^{47,48} alkene oligomerization,⁴⁹ alkane isomerization and cracking,⁵⁰ and isobutanol-isobutene Prins condensation.⁵¹

The excess Gibbs free energies for the detachment of zeolitic protons into the aqueous phase (ΔG_{excess}) (eq 7) at different extents of dissociation (α) are shown in Figure 5 for each

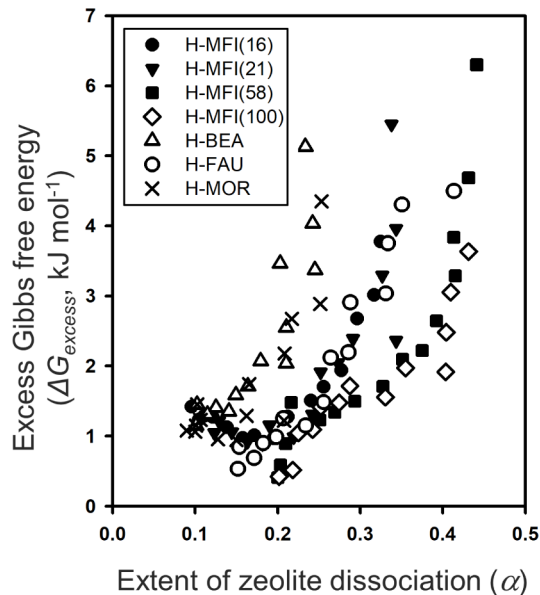


Figure 5. Measured excess Gibbs free energy (ΔG_{excess}) as a function of dissociation degree (α) for each zeolite at 298 K.

zeolite framework. On all samples, ΔG_{excess} values approach zero for low α values (the thermodynamically ideal case) and then increase sharply as the extent of dissociation increases (Figure 5). Specifically, ΔG_{excess} values increase most sharply as α values approach α_{max} (e.g., 0.49 for H-MFI(100); 0.28 for H-BEA), thus precluding any dissociation beyond α_{max} . The positive ΔG_{excess} values reflect the negative impact of charge accumulation within zeolite crystals on the detachment of additional protons. This ultimately precludes the detachment of all protons for all zeolites as extracrystalline $\text{H}_3\text{O}^+(\text{aq})$ ions. Such incomplete dissociation is reminiscent of the discrete step changes in dissociation constants ($K_{a1} > K_{a2} > K_{a3}$) for the sequential removal of each proton in polyprotic mineral or molecular acids, e.g., H_3PO_4 and $\text{H}_3\text{PW}_{12}\text{O}_{40}$.^{41,43} These latter systems also respond to the larger charge at the conjugate anion, but with an impact on energy that quantum mechanical in nature and specific to each solvated conjugate base; such

charges are present at the atomic scale of chemical bonds. For zeolite crystals acting as acids, the energy impact is predominantly classical, electrostatic in character, and relevant at the scale of zeolite crystals (10^2 – 10^4 nm); the Gibbs free energy of dissociation also changes continuously (instead of discretely, Figures 3 and S1), because of the large number of protons in each zeolite crystal and the much larger dimensions of the conjugate anion crystals.

The monotonic increase in ΔG_{excess} with extent of dissociation leads to larger activity coefficients for the conjugate anions ($\gamma_{(-z)} = \exp(-\Delta G_{\text{excess}}/RT)$) and consequently to smaller dissociation constants ($K_z \gamma_{(-z)}$) as α increases, in contrast with the discrete steps prevalent upon dissociation of polyprotic molecular and mineral acids. This merely reflects the very large number of protons in each zeolite “acid unit” (i.e., crystal). For instance, a $1 \mu\text{m}^3$ crystal of H-MFI with acid density of 1.6 BAS nm^{-3} contains $\sim 1.6 \times 10^9$ protons. At a dissociation extent of 0.01, the anionic charges at the conjugate base reside at a mean distance of 4.0 nm; the dissociation extent increases to 0.2 as the distance decreases to 1.5 nm. Such an increase of the α value with decreasing the distance continues, until reaching α_{max} when the anionic charges cannot get any closer. The much shorter distances among negative charges in “molecular” acids (e.g., ~ 0.3 nm in the two O^- atoms in HPO_4^{2-} anions) lead to drastic changes of dissociation energy and thus discrete decrease in dissociation constants with each additional removal of a proton.

The extent of dissociation of a zeolitic acid in aqueous systems is most sensitive to K_z , the intrinsic dissociation constant, and α_{max} , which accounts for the increase in the electrostatic work required to create additional charge as more protons are detached. The K_z values are similar on all zeolites examined, but α_{max} varies with the zeolite framework type and BAS density. In the next section, these K_z and α_{max} values are used to estimate the extracrystalline H_3O^+ concentrations at conditions where their direct measurement is still difficult (e.g., at higher hydrolysis temperatures of >473 K), and to relate rates of H_3O^+ -catalyzed hydrolysis of cellulose to the concentrations of hydronium ions present.

Acid-Catalyzed Hydrolysis of Cellulose by Extracrystalline $\text{H}_3\text{O}^+(\text{aq})$ Cations in Aqueous Suspensions of Acidic Zeolites. The dissociation of H-zeolites forms $\text{H}_3\text{O}^+(\text{aq})$ ions in the extracrystalline liquid phase. These hydronium ions must act as the mediating acid function in catalyzing the hydrolysis of cellulose, a molecule that cannot access protons in the intracrystalline regions, and specifically the kinetically relevant protonation and hydrolytic cleavage of C–O linkages in reactants. Such considerations indicate that hydrolysis rates must be proportional to the number of $\text{H}_3\text{O}^+(\text{aq})$ ions present in aqueous zeolite suspension. Confirming such a prediction requires either direct pH measurements at reaction temperatures (478 K) or extrapolation of the measured values of K_z and α_{max} determined at 298 K (Table 2) to such temperatures. The direct measurements are challenging and subject to pervasive artifacts, so the $\text{H}_3\text{O}^+(\text{aq})$ concentrations are estimated here by measuring the temperature dependence for K_z and α_{max} at lower and intermediate (and more accessible) temperatures.

Table 2 shows K_z values for H-MFI(16) that increased from $140 (\pm 8) \times 10^{-6}$ to $181 (\pm 21) \times 10^{-6}$ and α_{max} values that increased from $0.26 (\pm 0.02)$ to (0.46 ± 0.03) as temperatures increased from 274 to 313 K. These temperature effects on K_z

reflect the endothermic nature of zeolite dissociation ($\Delta H_{\text{d}}^\circ = 4.4 \pm 0.8 \text{ kJ mol}^{-1}$; Figure 6). The standard dissociation

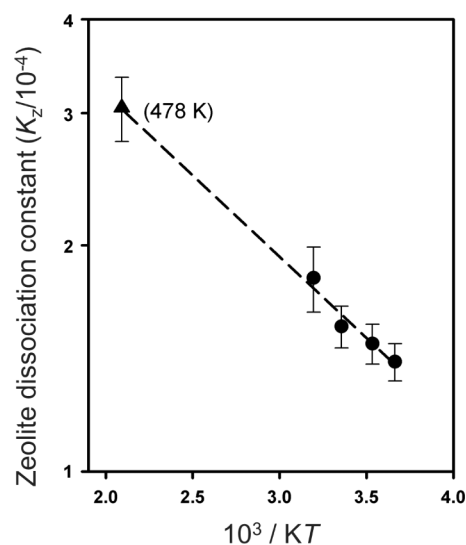


Figure 6. van't Hoff plot of the dissociation constant (K_z) of H-MFI(16). K_z is referenced to 1 mol/L H_3O^+ ion solution as the standard state. Dashed lines represent the results of a linear regression and the triangle the value of K_z estimated at 478 K.

entropy ($\Delta S_{\text{d}}^\circ$, obtained from Figure 6) is $-57 (\pm 15) \text{ J mol}^{-1} \text{ K}^{-1}$ (1 mol L^{-1} H_3O^+ standard state). When zeolite crystals are well-dispersed throughout the suspension, the dissociation of zeolitic acids is driven by the entropy gained upon detachment and the subsequent transfer of the bound protons to a well-mixed extracrystalline water phase as H_3O^+ ions ($\Delta S_{\text{d}} = 76 \pm 15 \text{ J mol}^{-1} \text{ K}^{-1}$); this leads to a $-T\Delta S_{\text{d}}$ term ($-22.6 (\pm 1.5) \text{ kJ mol}^{-1}$, 298 K) that exceeds the dissociation enthalpy of $4.4 (\pm 0.8) \text{ kJ mol}^{-1}$. The K_z values for H-MFI(16) at cellulose hydrolysis temperatures ($305 (\pm 30) \times 10^{-6}$, 478 K) were estimated by extrapolating the values measured at 274–313 K to the functional form of the expected van't Hoff relations (K_z vs $1/T$) (Figure 6). The same values of dissociation enthalpy ($4.4 \pm 0.8 \text{ kJ mol}^{-1}$) obtained on H-MFI(16) were used to obtain K_z values at 478 K for the other samples from the values measured directly at 298 K (Table 3), in light of their similar dissociation enthalpies.^{44,51,52}

The value of α_{max} (Table 2) also increased with temperature (0.27 ± 0.02 at 274 K; 0.46 ± 0.03 at 313 K; for H-MFI(16)). The interpretation (and prediction) of these effects and any plausible extrapolations of α_{max} to reaction temperatures

Table 3. Values of K_z and α_{max} for Each Zeolite Sample at the Temperature of Cellulose Hydrolysis Rate Measurements (478 K)

Zeolite	$K_z (\times 10^{-6})$	α_{max}^a
H-MFI(16)	305 ± 30	0.78 ± 0.03
H-MFI(21)	320 ± 30	0.77 ± 0.03
H-MFI(58)	330 ± 30	0.82 ± 0.04
H-MFI(100)	240 ± 25	0.81 ± 0.04
H-MOR	150 ± 15	0.69 ± 0.03
H-BEA	300 ± 30	0.66 ± 0.03
H-FAU	310 ± 30	0.76 ± 0.03

^aDetailed derivations are in Section S7.

requires insights about any temperature-dependent terms in eq 18,

$$\alpha_{\max} = \frac{1}{1 + \beta} = \frac{1}{1 + \frac{\rho_B q_c^2}{\epsilon_0 \epsilon_z k_B T} r_D (r_0 + r_D) \exp\left(-\frac{r_0}{r_D}\right)} \quad (18)$$

The permittivity of the wet zeolite (ϵ_z) contains contributions from the framework and the confined water molecules. The permittivity of silica is insensitive to temperatures (3–4 between 298 and 1300 K),⁵³ and siliceous zeolites exhibit even lower permittivity (1.5–2.5).^{54–56} The permittivity of water in confined spaces has been reported to be much lower than in bulk liquid water. For example, water confined between two plates separated by 1 nm has a ϵ_w value of about 2 in the out-of-plane direction at ambient temperature.⁵⁷ This value was used here for ϵ_z and assumed to be invariant with temperature in the range of interest (274–478 K).

The other temperature-dependent term (r_D ; Debye length) in eq 18 accounts for the screening of the negative charges by hydronium ions present within the crystallites; it was determined from measured α_{\max} values for different zeolites at 298 K and also for H-MFI(16) from 274 to 313 K (Table S1). The r_D values decreased with increasing ρ_B for these zeolites (Figure S2) and, in the case of H-MFI(16), decreased from 0.115 to 0.091 nm with temperature from 274 to 313 K (Figure S3). The Debye length for an electrolyte solution is given by

$$r_D = \sqrt{\frac{\epsilon_0 \epsilon_r k_B T}{2q_e^2 I}} \quad (19)$$

where ϵ_r is the relative permittivity of the surrounding medium (i.e., water for aqueous solution), and I is the ionic strength. To apply this equation to the micropore environment of zeolite, ϵ_r is replaced by ϵ_z , the relative permittivity of the zeolite crystal immersed in water, given the expression:

$$r_D = \sqrt{\frac{\epsilon_0 \epsilon_z k_B T}{2q_e^2 I}} \quad (20)$$

The extrapolation of r_D values to the temperature of catalytic interest (478 K) requires a relation between the ionic strength of the H_3O^+ ions and conjugate framework anions, in zeolite crystal (I , eq 10) and temperature. Using eq 20, the ionic strength for H-MFI(16) was determined from r_D values measured between 274 to 313 K, and extrapolated to 478 K (Figures S3b, S4). This ionic strength was used to estimate r_D and then the expected value of α_{\max} for this sample at 478 K. Then, r_D and α_{\max} were calculated for the other zeolites at 478 K using the r_D value for H-MFI(16) (Table 3), based on the assumption that temperature effects on ionic strength are similar on all zeolites (Section S7). This is a reasonable assumption because the temperature-dependence of ionic strength in zeolite voids is attributed to the temperature-dependent protonation and dissociation of zeolitic BAS (Scheme 1), a property of the zeolitic acid strength which is shown to be the same on all tested zeolites (i.e., the similar K_z values).

These estimates of K_z and α_{\max} values at 478 K (Table 3) allow estimates of the $\text{H}_3\text{O}^+(\text{aq})$ concentrations for each zeolite concentration at the conditions of cellulose hydrolysis (details in Section S8). Figure 7a shows that cellulose hydrolysis rates increase linearly with aqueous $\text{H}_3\text{O}^+(\text{aq})$

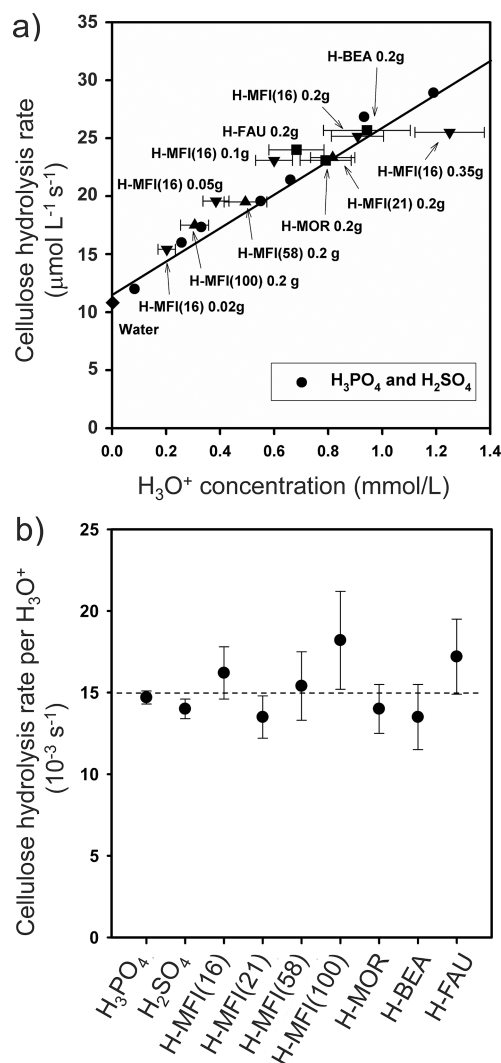


Figure 7. (a) Cellulose hydrolysis rate (given as number of cleaved glycosidic bonds per second) on different zeolites with different loadings and Si/Al ratios as a function of calculated hydronium ion (H_3O^+) concentrations; (b) cellulose hydrolysis rate per H_3O^+ ion for mineral acids and different zeolites. Reaction conditions: 478 K, 6 MPa H_2 , 40 g water, 1.0 g cellulose, 0.02 g 3% Ru/C, 20–30% conversion.

concentrations for all zeolites; these rate data lie along the same lines as for H_3PO_4 and H_2SO_4 mineral acids. This relation also includes the hydrolysis rates and $\text{H}_3\text{O}^+(\text{aq})$ concentrations for pure water. These linear trends, irrespective of the source of the $\text{H}_3\text{O}^+(\text{aq})$ ions shows that cellulose hydrolysis is catalyzed solely by hydronium ions in the extracrystalline aqueous phase.

The intrinsic competence of such species (but not their abundance) is independent of their provenance (or their concentration, as expected dilute character in the aqueous media). Cellulose hydrolysis rates “sense” the amount (per volume of water), identity, composition, and proton density of these acids only through their role in determining $\text{H}_3\text{O}^+(\text{aq})$ concentrations through their influence on the extent of dissociation of acidic zeolites. Turnover rates for cellulose hydrolysis (per $\text{H}_3\text{O}^+(\text{aq})$) are the same for all zeolites (with different frameworks and intracrystalline proton densities) and for mineral acids (Figure 7b). These similar turnover rates are expected from the similar properties and dilute nature of all

H_3O^+ species, irrespective of provenance; consequently, these results act, in turn, as confirmatory evidence for the validity and accuracy of the theoretical constructs used here to account for the effects of charge accumulation on the extent of dissociation. These formalisms can be extended, without modification, to the characterization and reactivity predictions for other solid acids (e.g., WO_3 , sulfonated carbons and resins, heteropoly acids) for which their mesoporous nature may lead to combined contributions from H_3O^+ ions within mesopores and throughout the bulk aqueous media for large molecules that are excluded, as in this case, from intracrystalline regions of zeolites. They are also expected to serve as essential and straightforward tools to characterize the dissociation properties of these solids, as well as those for microporous and mesoporous heterosilicates in which Al atoms are replaced by other trivalent cations (e.g., Ga, Fe, B).

The Recovery of Zeolite-Derived $\text{H}_3\text{O}^+(\text{aq})$ Upon Separating Solid Acids from Aqueous Suspensions.

The presence and role of detached $\text{H}_3\text{O}^+(\text{aq})$ ions in catalytic reactions may impact their full recovery as solids are recycled by filtration after reaction. The removal of such ions would lead, however, to the permanent formation of isolated solids and filtrate with large and equal negative and positive charges, respectively. In fact, the number of acid sites in H-MFI(16), as measured by NH_3 -TPD, is identical (0.86 vs 0.85 mmol g^{-1}) before and after vigorous stirring as a suspension in water for 10 h at 478 K and filtration. No detectable changes in cellulose hydrolysis rates (Figure 8a) are observed after five sequential reaction cycles (with intervening filtration). The pH of an

aqueous suspension of H-MFI(16) (28 g L^{-1}) was measured to be 3.08 while the pH of the supernatant solution after centrifugation was 6.60, a value similar to that of pure water in contact with ambient air (Figures 8b). These data show that none of the detached protons are permanently detached from zeolite crystals upon liquid–solid separation, making suspensions of zeolitic acids fully recyclable and reusable.

The entropy of mixing that enables the charge separation is lost upon removal of water from the suspension, leading to the reattachment of all protons to zeolite frameworks and allowing the indefinite separation and reuse of the solid acid catalysts. The $\text{H}_3\text{O}^+(\text{aq})$ ions return to the double layers and ultimately to the anionic framework as liquid water is removed by filtration and evaporation. In contrast with the situation for liquid acids, where the conjugate base is also solvated by the aqueous place, the crystalline conjugate anion is retained as the suspension is filtered and the H^+ ions are reattached to the anionic framework. Dissociation therefore becomes reversible upon physical separation of the solid from the liquid, making solid acids fully recoverable after their catalytic function is complete, in contrast with mineral and molecular acids.

CONCLUSIONS

Brønsted acid sites of zeolites dissociate to form the extracrystalline H_3O^+ ions in aqueous media and the conjugated anions in the zeolite frameworks. The H_3O^+ ions are fully recyclable and solely catalyze the hydrolysis of cellulose. The dissociation of zeolites, acting as weak polyprotic acids, reaches limited extents, irrespective of their framework structures and Si/Al ratios. Such incomplete dissociation is intrinsically imposed by the inhibiting effect of the electrostatic repulsion from the accumulated negative charges within the voids of the zeolites. Based on this dissociation model and the thermodynamic analysis, an equation for the dissociation extent of zeolites has been derived as a function of the extracrystalline H_3O^+ concentration and dissociation equilibrium constant. By this equation, the H_3O^+ concentrations in the aqueous phase for different zeolites have been calculated under the cellulose hydrolysis conditions, along with the known H_3O^+ concentrations of mineral acids, showing an excellent linearity with the measured cellulose hydrolysis rates. This work enables the direct comparison of zeolites and also other solid acids with mineral acids and the clarification of their intrinsic acidity in aqueous media especially involving in the reactions of cellulose and other bulky feedstocks (e.g., triglycerides, waste plastics etc.) that are not accessible to the internal acid sites.

ASSOCIATED CONTENT

Supporting Information

The Supporting Information is available free of charge at <https://pubs.acs.org/doi/10.1021/jacs.4c11705>.

Methods section, details on zeolite characterization, catalytic performance in cellulose hydrolysis, H_3O^+ concentration measurement, derivations of equations for cellulose hydrolysis rate, thermodynamic activity coefficient, electrostatic work to accumulate charges in zeolite and zeolite acid dissociation (PDF)

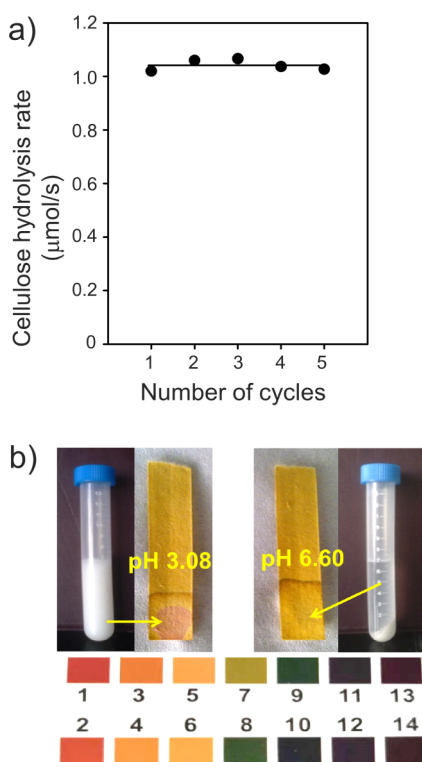


Figure 8. (a) Cellulose hydrolysis rates for five consecutive cycles. (b) pH values of aqueous suspension of H-MFI(16) under vigorous agitation and of its supernatant after centrifugation measured by pH meter (and conformed by pH strips) (0.2 g H-MFI(16), 7 mL H_2O , 298 K). Cellulose reaction conditions: 478 K, 30 min, 6 MPa H_2 , 40 g water, 1.0 g cellulose, 0.2 g H-MFI(16), 0.02 g 3%Ru/C.

AUTHOR INFORMATION

Corresponding Authors

Enrique Iglesia – Department of Chemical and Biomolecular Engineering, University of California at Berkeley, Berkeley, California 94720, United States; Davidson School of Chemical Engineering, Purdue University, West Lafayette, Indiana 47907, United States; Email: iglesia@purdue.edu

Haichao Liu – Beijing National Laboratory for Molecular Sciences, College of Chemistry and Molecular Engineering, Peking University, Beijing 100871, China; orcid.org/0000-0001-9175-3371; Email: hcliu@pku.edu.cn

Authors

Yue Liu – Beijing National Laboratory for Molecular Sciences, College of Chemistry and Molecular Engineering, Peking University, Beijing 100871, China; State Key Laboratory of Petroleum Molecular & Process Engineering, Shanghai Key Laboratory of Green Chemistry and Chemical Processes, School of Chemistry and Molecular Engineering, East China Normal University, Shanghai 200062, China; orcid.org/0000-0001-8939-0233

Chen Luo – Beijing National Laboratory for Molecular Sciences, College of Chemistry and Molecular Engineering, Peking University, Beijing 100871, China

Shuai Wang – State Key Laboratory for Physical Chemistry of Solid Surfaces, Collaborative Innovation Center of Chemistry for Energy Materials, and National Engineering Laboratory for Green Chemical Productions of Alcohols-Ethers-Esters, College of Chemistry and Chemical Engineering, Xiamen University, Xiamen 361005, China; orcid.org/0000-0002-4618-4162

Complete contact information is available at:

<https://pubs.acs.org/10.1021/jacs.4c11705>

Notes

The authors declare no competing financial interest.

ACKNOWLEDGMENTS

This work was supported by the National Natural Science Foundation of China (grant nos. 22032001, 21821004, 22472059, and 21690081), the National Key Research and Development Program of China (grant 2023YFA1506802), Natural Science Foundation of Shanghai (grant no. 23ZR1418800), and the Beijing National Laboratory for Molecular Sciences (grant BNLMS-CXXM-201905).

REFERENCES

- (1) Tanimu, A.; Tanimu, G.; Alasiri, H.; Aitani, A. Catalytic Cracking of Crude Oil: Mini Review of Catalyst Formulations for Enhanced Selectivity to Light Olefins. *Energy Fuels* **2022**, *36* (10), 5152–5166.
- (2) Zhao, R.; Khare, R.; Zhang, Y.; Sanchez-Sanchez, M.; Bermejo-Deval, R.; Liu, Y.; Lercher, J. A. Promotion of adsorptive and catalytic properties of zeolitic Brønsted acid sites by proximal extra-framework Si(OH)_x groups. *Nat. Catal.* **2023**, *6* (1), 68–79.
- (3) Wang, X.; Ma, Y.; Wu, Q.; Wen, Y.; Xiao, F.-S. Zeolite nanosheets for catalysis. *Chem. Soc. Rev.* **2022**, *51* (7), 2431–2443.
- (4) Cheng, K.; Smulders, L. C. J.; van der Wal, L. I.; Oenema, J.; Meeldijk, J. D.; Visser, N. L.; Sunley, G.; Roberts, T.; Xu, Z.; Daskoćil, E. Maximizing noble metal utilization in solid catalysts by control of nanoparticle location. *Science* **2022**, *377* (6602), 204–208.
- (5) Yang, Z.; Zhang, R.; Liu, R.; Zhang, S. Elucidating the zeolite particle size effect on butene/isobutane alkylation. *Ind. Eng. Chem. Res.* **2022**, *61* (2), 1032–1043.

- (6) Rastegar, S. F.; Sadovska, G.; Pilar, R.; Moravkova, J.; Kaucky, D.; Brabec, L.; Pastvova, J.; Sazama, P. Analysis of decisive structural parameters for alkylation of benzene with ethylene. *Appl. Catal., A* **2020**, *591*, 117379.

- (7) Pan, X.; Jiao, F.; Miao, D.; Bao, X. Oxide–zeolite-based composite catalyst concept that enables syngas chemistry beyond Fischer–Tropsch synthesis. *Chem. Rev.* **2021**, *121* (11), 6588–6609.

- (8) Jiao, F.; Bai, B.; Li, G.; Pan, X.; Ye, Y.; Qu, S.; Xu, C.; Xiao, J.; Jia, Z.; Liu, W. Disentangling the activity-selectivity trade-off in catalytic conversion of syngas to light olefins. *Science* **2023**, *380* (6646), 727–730.

- (9) Cheng, K.; Gu, B.; Liu, X.; Kang, J.; Zhang, Q.; Wang, Y. Direct and Highly Selective Conversion of Synthesis Gas into Lower Olefins: Design of a Bifunctional Catalyst Combining Methanol Synthesis and Carbon–Carbon Coupling. *Angew. Chem., Int. Ed.* **2016**, *55* (15), 4725–4728.

- (10) Han, S.; Fan, D.; Chen, N.; Cui, W.; He, L.; Tian, P.; Liu, Z. Efficient Conversion of Syngas into Ethanol by Tandem Catalysis. *ACS Catal.* **2023**, *13* (16), 10651–10660.

- (11) Wu, X.; Wei, Y.; Liu, Z. Dynamic Catalytic Mechanism of the Methanol-to-Hydrocarbons Reaction over Zeolites. *Acc. Chem. Res.* **2023**, *56* (14), 2001–2014.

- (12) Kirchberger, F. M.; Liu, Y.; Plessow, P. N.; Tonigold, M.; Studt, F.; Sanchez-Sanchez, M.; Lercher, J. A. Mechanistic differences between methanol and dimethyl ether in zeolite-catalyzed hydrocarbon synthesis. *Proc. Natl. Acad. Sci. U. S. A.* **2022**, *119* (4), No. e2103840119.

- (13) Chen, W.; Tarach, K. A.; Yi, X.; Liu, Z.; Tang, X.; Góra-Marek, K.; Zheng, A. Charge-separation driven mechanism via acylium ion intermediate migration during catalytic carbonylation in mordenite zeolite. *Nat. Commun.* **2022**, *13* (1), 7106.

- (14) Veltý, A.; Corma, A. Advanced zeolite and ordered mesoporous silica-based catalysts for the conversion of CO₂ to chemicals and fuels. *Chem. Soc. Rev.* **2023**, *52* (5), 1773–1946.

- (15) Wen, C.; Jiang, J.; Chihli, C.; Tian, Z.; Xu, X.; Wu, J.; Wang, C.; Ma, L. Single-Step Selective Conversion of Carbon Dioxide to Aromatics over Na-Fe₃O₄/Hierarchical HZSM-5 Zeolite Catalyst. *Energy Fuels* **2020**, *34* (9), 11282–11289.

- (16) Dong, Z.; Chen, W.; Xu, K.; Liu, Y.; Wu, J.; Zhang, F. Understanding the Structure–Activity Relationships in Catalytic Conversion of Polyolefin Plastics by Zeolite-Based Catalysts: A Critical Review. *ACS Catal.* **2022**, *12* (24), 14882–14901.

- (17) Duan, J.; Chen, W.; Wang, C.; Wang, L.; Liu, Z.; Yi, X.; Fang, W.; Wang, H.; Wei, H.; Xu, S. Coking-Resistant Polyethylene Upcycling Modulated by Zeolite Micropore Diffusion. *J. Am. Chem. Soc.* **2022**, *144* (31), 14269–14277.

- (18) Woolery, G. L.; Kuehl, G. H.; Timken, H. C.; Chester, A. W.; Vartuli, J. C. On the nature of framework Bronsted and Lewis acid sites in ZSM-5. *Zeolites* **1997**, *19* (4), 288–296.

- (19) Wouters, B. H.; Chen, T. H.; Grobet, P. J. Reversible tetrahedral-octahedral framework aluminum transformation in zeolite Y. *J. Am. Chem. Soc.* **1998**, *120* (44), 11419–11425.

- (20) Kuehl, G. H.; Timken, H. K. C. Acid sites in zeolite Beta: Effects of ammonium exchange and steaming. *Microporous Mesoporous Mater.* **2000**, *35*–36, 521–532.

- (21) Li, C.; Xu, G.; Wang, C.; Ma, L.; Qiao, Y.; Zhang, Y.; Fu, Y. One-pot chemocatalytic transformation of cellulose to ethanol over Ru-WO_x/HZSM-5. *Green Chem.* **2019**, *21* (9), 2234–2239.

- (22) Sreekantan, S.; Pratap Singh, C.; Krishnamurthy, S.; Marimuthu, B. Investigation of the Effect of Zeolite Supports and the Role of W-Species for One-Pot Catalytic Conversion of Cellulose to Ethylene Glycol: Theoretical & Experimental Studies. *Chem. -Asian J.* **2023**, *18* (4), No. e202201202.

- (23) Xu, Z.-M.; Luo, J.-Y.; Huang, Y.-B. Recent advances in the chemical valorization of cellulose and its derivatives into ester compounds. *Green Chem.* **2022**, *24* (10), 3895–3921.

- (24) Luo, C.; Wang, S. A.; Liu, H. C. Cellulose conversion into polyols catalyzed by reversibly formed acids and supported ruthenium

- clusters in hot water. *Angew. Chem., Int. Ed.* **2007**, *46* (40), 7636–7639.
- (25) Shrotri, A.; Kobayashi, H.; Fukuoka, A. Air Oxidation of Activated Carbon to Synthesize a Biomimetic Catalyst for Hydrolysis of Cellulose. *ChemSuschem* **2016**, *9* (11), 1299–1303.
- (26) Zeng, M.; Pan, X. Insights into solid acid catalysts for efficient cellulose hydrolysis to glucose: Progress, challenges, and future opportunities. *Catal. Rev.* **2022**, *64* (3), 445–490.
- (27) Klemm, D.; Heublein, B.; Fink, H.-P.; Bohn, A. Cellulose: Fascinating Biopolymer and Sustainable Raw Material. *Angew. Chem., Int. Ed.* **2005**, *44* (22), 3358–3393.
- (28) Fukuoka, A.; Dhepe, P. L. Catalytic conversion of cellulose into sugar alcohols. *Angew. Chem., Int. Ed.* **2006**, *45* (31), S161–S163.
- (29) Smallwood, L. M.; White, R. L. Zeolite catalyzed hydrolysis in aqueous and ionic liquid media. *J. Biomass Biofuel* **2014**, *1*, 1–7.
- (30) Cai, H.; Li, C.; Wang, A.; Xu, G.; Zhang, T. Zeolite-promoted hydrolysis of cellulose in ionic liquid, insight into the mutual behavior of zeolite, cellulose and ionic liquid. *Appl. Catal., B* **2012**, *123–124*, 333–338.
- (31) Geboers, J.; Van de Vyver, S.; Carpentier, K.; Jacobs, P.; Sels, B. Efficient hydrolytic hydrogenation of cellulose in the presence of Ru-loaded zeolites and trace amounts of mineral acid. *Chem. Commun.* **2011**, *47* (19), 5590–5592.
- (32) Vjunov, A.; Derewinski, M. A.; Fulton, J. L.; Camaioni, D. M.; Lercher, J. A. Impact of Zeolite Aging in Hot Liquid Water on Activity for Acid-Catalyzed Dehydration of Alcohols. *J. Am. Chem. Soc.* **2015**, *137* (32), 10374–10382.
- (33) Liu, Y.; Vjunov, A.; Shi, H.; Eckstein, S.; Camaioni, D. M.; Mei, D. H.; Barath, E.; Lercher, J. A. Enhancing the catalytic activity of hydronium ions through constrained environments. *Nat. Commun.* **2017**, *8*, 14113.
- (34) Shi, H.; Eckstein, S.; Vjunov, A.; Camaioni, D. M.; Lercher, J. A. Tailoring nanoscopic confines to maximize catalytic activity of hydronium ions. *Nat. Commun.* **2017**, *8*, 15442.
- (35) Parks, G. A. Review Isoelectric points of solid oxides, solid hydroxides, and aqueous hydroxo complex systems. *Chem. Rev.* **1965**, *65*, 177–198.
- (36) Chen, Y. H.; Huang, S. J.; Wan, B. Z. Reversal of Zeta Potential of Proton-Type Zeolite Y after Surface Modifications in Sodium Ion Aqueous Solutions. *Ind. Eng. Chem. Res.* **2016**, *55* (7), 1921–1928.
- (37) Marshall, W. L.; Franck, E. U. Ion Product of Water Substance, O-Degrees-C-1000-Degrees-C, 1–10,000 bar - New International Formulation and Its Background. *J. Phys. Chem. Ref. Data* **1981**, *10* (2), 295–304.
- (38) Liu, Y.; Chen, L.; Zhang, W.; Liu, H. Recyclable Cu salt-derived Brønsted acids for hydrolytic hydrogenation of cellulose on Ru catalyst. *CCS Chem.* **2022**, *4* (9), 3162–3169.
- (39) Deng, T.; He, X.; Liu, H. Insights into the Active Acid Sites for Isosorbide Synthesis from Renewable Sorbitol and Cellulose on Solid Acid Catalysts. *Chem. Res. Chin. Univ.* **2022**, *38* (1), 257–264.
- (40) Otomo, R.; Yokoi, T.; Tatsumi, T. Synthesis of isosorbide from sorbitol in water over high-silica aluminosilicate zeolites. *Appl. Catal., A* **2015**, *505*, 28–35.
- (41) Mesmer, R. E.; Baes, C. F. Phosphoric Acid Dissociation Equilibria Aqueous Solutions to 300 degrees C. *J. Solution Chem.* **1974**, *3* (4), 307–322.
- (42) Marshall, W. L.; Jones, E. V. 2nd Dissociation Constant of Sulfuric Acid from 25 to 350 Degrees Evaluated from Solubilities of Calcium Sulfate in Sulfuric Acid Solutions. *J. Phys. Chem.* **1966**, *70* (12), 4028–4040.
- (43) Kozhevnikov, I. V. E. Advances in catalysis by heteropolyacids. *Russ. Chem. Rev.* **1987**, *56* (9), 811.
- (44) Jones, A. J.; Iglesia, E. The Strength of Brønsted Acid Sites in Microporous Aluminosilicates. *ACS Catal.* **2015**, *5* (10), 5741–5755.
- (45) Rybicki, M.; Sauer, J. Acid strength of zeolitic Brønsted sites—Dependence on dielectric properties. *Catal. Today* **2019**, *323*, 86–93.
- (46) Deshlahra, P.; Iglesia, E. Reactivity descriptors in acid catalysis: Acid strength, proton affinity and host–guest interactions. *Chem. Commun.* **2020**, *56* (54), 7371–7398.
- (47) Jones, A. J.; Zones, S. I.; Iglesia, E. Implications of Transition State Confinement within Small Voids for Acid Catalysis. *J. Phys. Chem. C* **2014**, *118* (31), 17787–17800.
- (48) Jones, A. J.; Carr, R. T.; Zones, S. I.; Iglesia, E. Acid strength and solvation in catalysis by MFI zeolites and effects of the identity, concentration and location of framework heteroatoms. *J. Catal.* **2014**, *312*, 58–68.
- (49) Sarazen, M. L.; Dorskocil, E.; Iglesia, E. Effects of Void Environment and Acid Strength on Alkene Oligomerization Selectivity. *ACS Catal.* **2016**, *6* (10), 7059–7070.
- (50) Noh, G.; Zones, S. I.; Iglesia, E. Consequences of acid strength and diffusional constraints for alkane isomerization and β -scission turnover rates and selectivities on bifunctional metal-acid catalysts. *J. Phys. Chem. C* **2018**, *122* (44), 25475–25497.
- (51) Wang, S.; Iglesia, E. Catalytic diversity conferred by confinement of protons within porous aluminosilicates in Prins condensation reactions. *J. Catal.* **2017**, *352*, 415–435.
- (52) Herrmann, S.; Iglesia, E. Elementary steps in acetone condensation reactions catalyzed by aluminosilicates with diverse void structures. *J. Catal.* **2017**, *346*, 134–153.
- (53) Yuan, J.; Wen, B.; Hou, Z.-L.; Lu, M.-M.; Cao, W.-Q.; Ba, C.; Fang, X.-Y.; Cao, M.-S. High-temperature permittivity and data-mining of silicon dioxide at GHz band. *Chin. Phys. Lett.* **2012**, *29* (2), 027701.
- (54) Larlus, O.; Mintova, S.; Valtchev, V.; Jean, B.; Metzger, T.; Bein, T. Silicalite-1/polymer films with low-k dielectric constants. *Appl. Surf. Sci.* **2004**, *226* (1–3), 155–160.
- (55) Li, Z.; Johnson, M. C.; Sun, M.; Ryan, E. T.; Earl, D. J.; Maichen, W.; Martin, J. I.; Li, S.; Lew, C. M.; Wang, J. Mechanical and Dielectric Properties of Pure-Silica-Zeolite Low-k Materials. *Angew. Chem., Int. Ed.* **2006**, *45* (38), 6329–6332.
- (56) Tiriolo, R.; Rangnekar, N.; Zhang, H.; Shete, M.; Bai, P.; Nelson, J.; Karapetrova, E.; Macosko, C. W.; Siepmann, J. I.; Lamanna, E.; et al. Sub-Micrometer Zeolite Films on Gold-Coated Silicon Wafers with Single-Crystal-Like Dielectric Constant and Elastic Modulus. *Adv. Funct. Mater.* **2017**, *27* (25), 1700864.
- (57) Fumagalli, L.; Esfandiari, A.; Fabregas, R.; Hu, S.; Ares, P.; Janardanan, A.; Yang, Q.; Radha, B.; Taniguchi, T.; Watanabe, K.; et al. Anomalously low dielectric constant of confined water. *Science* **2018**, *360* (6395), 1339–1342.